Metal (hydr)oxide surface precipitates and their effects on potassium sorption

SCHOLARONE™
Manuscripts

1
2
3
4
5
6
7
8
9
10
11
12
13
14
15
16
17
18
19
20
21
22
23
24
25
26
27
28
29
30
31
32
33
34
35
36
37
38
39
40
41
42
43
44
45
46
47
48
49
50
51
52
53
54
55
56
57
58
59
60

Metal (hydr)oxide surface precipitates and their effects on potassium sorption

Author names and affiliations

Thanh Quang Pham [a, b], Aakriti Sharma [a**], Katherine Coyle [a, c], Katie Lewis [a], Matthew G. Siebecker [a*]

Email: thanh.pham@ttu.edu, aakrisha@ttu.edu, katherine.coyle@ttu.edu, katie.lewis@ttu.edu, matthew.siebecker@ttu.edu.

[a] Department of Plant and Soil Science, Texas Tech University, 2911 15th Street, Suite 122, Lubbock, TX 79409, USA.

[b] Department of Chemical Engineering, Texas Tech University, P.O. Box 43121, Lubbock, Texas, 79409, USA.

[c] Department of Geosciences, Texas Tech University, 1200 Memorial Circle, Lubbock, Texas 79409, USA.

*Corresponding author

Matthew G. Siebecker, Email: matthew.siebecker@ttu.edu, Phone: +1 (806) 834-0266. FAX: +1 (806) 742-0775

**Co-corresponding author

Aakriti Sharma, Email: aakrisha@ttu.edu, Phone: +1 (919) 916-7626

Abstract

Surface precipitation has been shown to occur on rapid time scales in clay and metal oxide mineral systems. The formation of surface precipitates is hypothesized to present new potential sorption sites for potassium (K), where K can become incorporated into newly formed interlayer spaces (e.g., between tetrahedral-octahedral-tetrahedral stacked sheets). The objective of this study is to determine the effects of newly formed mineral surface precipitates on K sorption. Potassium adsorption experiments were conducted by utilizing Al_2O_3 and SiO_2 sorbents in the presence of various cations (magnesium, zinc, and nickel) that helped to catalyze the formation of surface precipitates. Dissolved concentrations of elements were monitored via inductively coupled plasma optical emission spectrometry (ICP-OES). Solids were characterized via X-ray diffraction (XRD), and K surface complexation was analyzed via X-ray absorption near edge structure (XANES) spectroscopy. X-ray diffraction analysis indicated bayerite, layered double hydroxides (LDH), and silicated LDH were formed as reaction products, thus creating new surface sites for potential K adsorption. The presence of Si increased K adsorption perhaps due to its role in the formation of LDH surface precipitates. When the differences between observed and theoretical surface area normalized K sorption densities were averaged, a 31% increase in K adsorption was observed in the presence of Si. XANES analysis indicated that the binding mechanism of K to Si is different than that of K to Al, perhaps due to the presence of inner-sphere complexation of K to Al-oxide. Samples reacted for one month versus one week yielded more intense XANES post-edge peaks which indicated that the K sorption complex changes over time. Overall, our findings provide novel insights into the mechanisms of K fixation in soil and has high implication in providing improved K fertilizer recommendation to growers.

Environmental Significance

Potassium (K) is an essential nutrient for crop production, yet bioavailability of K remains problematic. This presents a major challenge for growers in terms of economic crop production. Part of this problem is due to the lack of fundamental understanding for how K can be sequestered in soil. In general, K fixation occurs due to the collapse of the clay mineral structure; however, we report a novel pathway for K fixation at short timescales. Metal ions catalyze the formation of new surface precipitates in Al- and Si-oxide mineral systems, and these surface precipitates can enhance K sorption. These findings provide an improved fundamental understanding for K surface chemical reactions and will help to improve recommendations for K fertilizer application.

1. Introduction

Bioavailability of potassium (K) in soil is critical for proper plant growth and yield [1-4]. While soils may contain high levels of K, plants may still suffer from K deficiency if soil K is inaccessible to plants [5-9]. Therefore, understanding novel pathways for K fixation in soil is important for effective management of K in soil. Potassium chemistry in soil has been studied since the early 20th century [10], and in-depth discussions on the physical chemistry of K in soil, including its release, chemical equilibria, and kinetics have been previously documented [11, 12].

However, it is the rapid formation of new minerals such as metal hydroxides that are the basis for reexamination of the binding of the K in soil and clay mineral systems. It is now well established that several transition metal cations (e.g., Zn, Ni) can form mixed metal Al-hydroxide surface precipitates on Al oxides and Al-rich soil clays, which can readily incorporate Si to form layered-silicate structures [13-15]. Clay interlayer spaces are well known to sequester K

(e.g., illite). It has been shown that the exchange of K from K-rich minerals such as vermiculite

or micaceous minerals tends to be slow; the selectivity in the interlayer spaces of micaceous

minerals is more restrictive than vermiculite because the micaceous minerals are more selective

for K [16]. More K can be bound to micaceous minerals than vermiculite phases. Regardless, it is

the interlayer spaces that play the key role in retaining K as an adsorbed species versus allowing

it to be mobile in soil porewater. The formation of new interlayer spaces and their potential to

adsorb K during and after surface precipitation has not been examined previously.

The interlayer spaces also play a key role in soil K desorption, which is critical to supply

plant bioavailable K. Because of the collapsing interlayer spaces in vermiculite clay minerals, the

diffusion rate of K desorption is slower than for K adsorption [17]. During K adsorption, K

essentially partitions between the dissolved soluble phase (i.e., hydrated with water molecules),

as an adsorbed phase (i.e., bound directly to the solid), or an intermediate phase where there is

some inner-sphere complexation of K to the solid while part of the K ion (K^+) remains hydrated

[18]. When K is located in the interlayer spaces of clay minerals, the electrostatic forces between

K^+ and the silicate layers are greater than the coulombic forces between the K^+ and the water in

its sphere of hydration [19]. This causes the interlayer spaces to partially collapse around K.

To address the problem of potassium fixation in soil, this study aims to understand at a

fundamental level the potentially overlooked mechanisms by which K can become sequestered in

soil and mineral system. Specifically, the incorporation of K into newly formed surface

precipitates is examined. Surface precipitation of metal hydroxides has been shown to occur very

quickly in mineral systems; and the surface precipitates can quickly incorporate dissolved silicon

to form silicated-layered minerals, similar to phyllosilicates [14, 20-22]. These types of minerals are

generally referred to as layered double hydroxides (LDH). They are stacks of octahedral layers

formed by edge-sharing octahedra, and they accommodate +2 and +3 valence metals [13]. The role

that metal hydroxides play in soils is significant, impacting numerous sorption/desorption

reactions of trace metals and plant nutrients [23]. Metal dissolution followed by hydrolysis is a

dominant mechanism for the formation of amorphous metal hydroxides [13]. For example, the

formation of LDHs involves a dissolution-reprecipitation process, where the dissolution of Al

has been proposed to be the rate limiting step for LDH formation; in the presence of silicate, the

coprecipitation of Zn and Al leads to a poorly crystallized hydrotalcite-like phase, whereas in the

absence of silicate, the precipitate is more crystalline [24]. Thus, in addition to metal hydrolysis,

the presence of dissolve anions such as silicate also impact nutrient sorption. The positive charge

of the LDH is readily satisfied by negatively charged dissolved silica (H_4SiO_4), which can

become incorporated into the interlayer spaces [15]. Therefore, the positive charge can be quickly

neutralized, resulting in phyllosilicate-type mineral as a newly formed surface precipitate. The

formation of these types of precipitates is hypothesized to present new potential binding sites for

K into newly formed mineral interlayer spaces.

        The specific objective of this study is to identify the effects that newly formed mineral

surface precipitates have on K sorption. To carry out this study, K sorption on γ-Al_2O_3 and SiO_2

was conducted in the presence of additional dissolved cations (Zn, Ni, and Mg), under different

reaction times. We chose γ-Al_2O_3 because of the high solubility of this mineral, as mineral

dissolution plays an important role in formation of surface precipitates [24]. As discussed above,

Zn and Ni have been shown to catalyze the formation of mixed metal Al-hydroxides, and the

presence of dissolved silica from SiO_2 plays an important role in the formation of silicated

layered minerals. Additionally, because Mg does not generally catalyze the formation of surface

precipitates (although it can form hydrotalcite minerals under co-precipitation conditions), we

considered the magnesium treatment as a comparison to analyze our systems in the absence of

minerals formed (i.e., surface precipitates). Thus, these minerals and cations were carefully

selected for our study. A combination of wet chemical, spectroscopic, and microscopic

techniques was applied to quantify and describe K sorption mechanisms and surface precipitate

formation. Aqueous analysis was carried out via Inductively Coupled Plasma - Optical Emission

Spectrometry (ICP-OES). Surface precipitates were identified via X-ray diffraction (XRD), and

X-ray absorption near edge structure (XANES) spectroscopy was used to identify changes in K

coordination and characterize the potential incorporation of K into surface precipitates.

2. Experimental Methods

2.1 Adsorption experiments

Adsorption experiments were carried out to identify the K sorption capacity of two oxide

minerals. Gamma (γ) Al_2O_3 and SiO_2 oxides were purchased from SkySpring Nanomaterials,

Inc. (Houston, TX). The γ-alumina (product 1333DL) has an average particle size of 15 nm and

an average surface area of greater than 400 m^2 g^{-1}. The SiO_2 (6707NM) has an average particle

size of 10-20 nm and an average surface area of 640 m^2 g^{-1}. These minerals were selected

because Al and Si oxides are prevalent in soils and both are known to participate in the formation

of surface precipitates in the presence of dissolved cations [24, 25].

Eleven samples were prepared that contained different combinations of mineral(s) and

cations (e.g., Mg, Ni, and Zn) in 50 mL polypropylene centrifuge tubes. Each samples contained

either 0.1 g of Al_2O_3 or SiO_2, or an equal mix of both minerals, and 3 mM Mg, Zn, or Ni nitrate,

along with 1 mM KNO_3. The samples were prepared in 10 mM $NaNO_3$ background electrolyte

and a 50 mM HEPBS buffer solution adjusted to pH 8.5 was also added to each sample to

maintain the pH at 8.5. The samples were reacted at pH 8.5 to catalyze the formation of surface precipitates as it is known that surface precipitate formation increases with pH [24]. Additionally, the soils in West Texas which are used for cotton production can be highly alkaline (up to pH 8.5) in subsoil layers [26], and thus the pH selected for our study is relevant to natural environmental conditions. The total volume of reaction was 40 mL. Each set of samples were reacted for 1-week and 1-month at 200 rpm using the VWR Advanced Digital Shaker. All samples were run in triplicate. After shaking for the desired time, the pH of samples was measured. The samples were then centrifuged at 9250 rpm for 15 minutes using Thermo Scientific Multifuge X3R Refrigerated Centrifuge to separate solids from the solutions and the supernatants were collected into new 50 mL tubes. The solids were further rinsed with 5 mL of DI water and centrifuged to remove any K that was bound via outer-sphere complexation. The supernatants after the rinse were also collected and added to the 50 mL tubes and filtered through 0.22 μm nylon syringe filters. Finally, 9.8 mL aliquots of filtrates were acidified with 0.2 mL of concentrated HNO_3 and analyzed using ICP-OES.

2.2 Sample characterization

The acidified supernatants were analyzed via ICP-OES to determine the amount of K, Al, Si, Ni, and Zn that remained in the liquid phase, which represent the dissolved cations that were not bound into mineral phases. Based on the amount of K added and the amount of K detected in the liquid phase post reaction, the total amount of K bound to the solid (q in mg K kg mineral^{-1}) was determined via q = $(C_0*V_0-C_f*V_f)/m$), where C_0 and C_f are the initial and final concentrations (mg L^{-1}) of the sorptive ions, respectively, V_0 and V_f are the initial and final volumes of the solution (L), respectively, and m is the mass of the added mineral phases.

After the reactions were completed, the solids were isolated and freeze-dried to determine any changes in the mineralogy of the samples. The solid samples were analyzed on an XRD Miniflex instrument to determine if the formation of new minerals occurred. The sample were scanned from 5 to 80° 2θ with a counting time of 0.4 s at each step. The XRD data analyses were conducted using software packages Match! (Crystal Impact) and Jade from MDI™. The Relative Intensity Ratio (RIR) method was used to semi-quantitatively determine the mineralogy. The solid samples were also analyzed at higher resolution using Hitachi H-9500 transmission electron microscopy (TEM) equipped with energy dispersive X-ray (EDX) spectrometer to determine any changes in mineralogy and identify surface precipitates in the reacted samples. The TEM images and the EDX spectra were collected on the well dispersed non-reacted samples and samples containing Zn that were reacted for one month. The d-spacing value of the lattice fringes in the TEM images were used to determine if any new precipitates were formed, and the EDX data were used to corroborate the findings.

2.3 X-ray absorption spectroscopy

Potassium K-edge XANES spectra were collected at beamline 4-3 at the Stanford Synchrotron Radiation Lightsource (SSRL) (Menlo Park, CA) to determine K speciation on the solid samples. The samples for XANES analysis were prepared by packing freeze-dried solid sample in custom built Al sample holders specific to beamline 4-3. The front side of the sample holder was covered with Prolene XRF film and samples were sealed from the back by Kapton tape. Caution was used to prevent cross contamination between the samples. Multiple scans were collected and averaged together to increase the signal to noise ratio. Samples were calibrated to 3610 eV, which is the E0 of a solid phase KCl standard [27]. Data were collected in fluorescence

mode using a seven element Vortex detector. The pre-edge region was collected from -150 to -

120 below E0 at a 5 eV step size. A smaller step size of 0.3 eV was used across the edge region

(-20 to 30 eV). XANES data were processed using the Athena [28] and Sixpack [29] software

packages.

3. Results and Discussion

3.1 Impacts of Mg, Zn, and Ni on mineral transformation

SiO_2 and Al_2O_3 were reacted with K in presence or absence of additional cations such as

Mg, Zn, or Ni at both 1-week (1W) and 1-month (1M) time periods at room temperature. The

XRD patterns of the samples reacted with K and Mg are reported in Figure 1. The XRD patterns

for the non-reacted samples (i.e. the dry powder (DP) samples) are presented at the bottom of the

figure, which are used for comparing reacted samples. When SiO_2 was reacted with K and Mg

for either 1-week or 1-month, no visible changes in the XRD pattern could be observed. The

mixed system, i.e., $SiO_2+Al_2O_3$ (SiAl) reacted with K and Mg, and the mixed system with no

additional cations reacted for 1-week also exhibited XRD spectra similar to the dry powder (non-

reacted) samples. Whereas, the mixed SiAl system with no additional cation reacted for 1-month

resulted in several new peaks at about 18.7, 19.2, 20.7, 28.3, 41.0, and 53.6° 2θ. All of those

peaks can be indexed to bayerite. Additionally, K and Mg reacted with single Al_2O_3 system

resulted in new peaks at approximately 18.8 and 20.7 ° 2θ, and those peaks can be indexed to

both bayerite and gibbsite. All the other major peaks (e.g., at 32.5, 37.5, 40, 46, 61, and 67.2 °

2θ) all correspond to ɣ-Al_2O_3 (gamma alumina).

However, the addition of Zn catalyzed the formation of new mineral precipitates in both

the mixed oxide and single Al oxide systems (Figure 2). When SiO_2 is reacted with Zn for either

1-week or 1-month, there are no visible changes in the XRD pattern, indicating that no new

mineral precipitates formed. Whereas, the Al_2O_3 samples reacted with Zn for 1-week and 1-month showed several noticeable new peaks at 12.1, 18.7, 19.2, 20.7, 23.9, 28.2, 34.2, 35, 39.6, 40.8, 53.5, 57.9, 60.7, 62.1, 64.1, and 71.2° 2θ. The XRD data show newly formed bayerite which corresponded to peaks at 18.7, 20.7, 28.2, 39.6, 53.5° 2θ. The other peaks can be indexed to zaccagnaite, a mineral that belongs to hydrotalcite-manasseite group, and whose structure is characterized by brucite-like layers with Al and Zn and an interlayer of carbonate [30], which is the same as AlZn LDH. The 1-month peaks are higher than those of the 1-week, indicating that mineral precipitation continues to occur over time. The mixed oxide samples reacted with Zn also form new XRD peaks at about 12, 23.7, 34.1, 35, 39.5, 47, 60.5, 61.9, and 66° 2θ, which can be primarily indexed to zaccagnaite. This indicates that the presence of Si does not completely inhibit the formation of LDH precipitates. The formation of new precipitates in the single and mixed Al systems containing Zn is also indicated by the TEM images (Figure S1-S5 in the SI) as discussed below.

To corroborate the findings from XRD, TEM analysis was undertaken on select samples, which further aided to describe the morphology and elemental distribution of the newly formed surface precipitates. Figure S1 in the Supporting Information shows the TEM images of non-reacted (pristine) ɣ-Al_2O_3 and SiO_2, where ɣ-Al_2O_3 is crystalline in nature as indicated by the presence of lattice fringes (d-spacing = 4.6 Å) at high resolution (Figure S1b), and SiO_2 is amorphous in nature. Figure S2 and S3 shows the low magnification and high resolution TEM images of AlZn1M and SiAlZn1M. These images show the presence of newly formed surface precipitate, as indicated by the darker regions, which was indexed to be zaccagnaite. The d-spacing value of the lattice fringes in the darker regions was found to be 2.5 and 2.6 Å, which corresponds to that of zaccagnaite, and the d-spacing value of 4.6 Å or 2.8 Å in the lighter region

corresponds to ɣ-Al_2O_3. The EDX spectra collected to assess elemental distribution showed that the darker region was Zn-rich, compared to regions that are predominantly ɣ-Al_2O_3 or SiO_2 (Figure S4 and S5), which further supported the formation of zaccagnaite on the ɣ-Al_2O_3 substrate.

Similar to the Zn-system, when Ni is added to each oxide system, new peaks can be observed in the XRD pattern (Figure 3). When SiO_2 is reacted with Ni for either 1-week or 1-month, two new peaks are observed. These peaks are similar to silicated-$Ni(OH)_2$ [14]. This is different than the Mg and Zn systems where no additional peaks were observed when Mg and Zn were reacted with SiO_2. The reaction time did not significantly affect the formation of silicated-$Ni(OH)_2$ on the SiO_2 indicated by the similar intensities of the peaks. These results indicate that Ni has a different behavior than Zn and Mg with respect to formation of surface precipitates in the Si system. The Zn and Mg ions did not seem to catalyze any observable silicate/hydroxide peaks based on XRD. This indicates that while Ni and Zn were both hypothesized to form some type of silicate hydroxide in the Si system, Ni appears to be more reactive than Zn in the dissolution and reprecipitation of silicate.

On the other hand, Al_2O_3 samples reacted with Ni for 1 month formed 12 new peaks which exhibited variety of wide and sharp features. The new peaks at 19.2, 20.7, 28.3, 41, 53.5, 58, 59.6, and 71.1° 2θ can all be indexed to bayerite. These peaks are characteristically sharper than the new peaks at 11.8, 22.2, 35, and 61.5° 2θ which can also be indexed to NiAl LDH [15]. The height of the bayerite peaks also significantly increase from the 1-week to the 1-month reaction time. The reacted mixed oxide samples also show the presence of newly formed LDH peaks, but the peak intensities do not increase over time. Importantly, in the presence of Si, bayerite does not form over time. This indicates that Si inhibits the formation of bayerite,

perhaps due to the role of Si in preventing surface precipitate crystallization [24]. This phenomenon

has also been observed by others; for example, when silicon is present in the sorbent (e.g., with

pyrophyllite or kaolinite), dissolved silicate can enter the interlayer space of surface precipitates,

and when this occurs, the surface precipitates tend to be more amorphous, lacking long range

order and not detectable by XRD [31].

The objective of adding cations like Mg, Zn, and Ni was to catalyze the formation of

surface precipitates [32, 33], and we hypothesized that surface precipitates which have layered

structure will provide additional sorption sites for K to bind in the interlayer spaces. In all of the

systems studied, bayerite was identified as a new precipitate forming in the Al_2O_3 systems. This

occurred in the presence of Mg, Zn, or Ni (Figure 1, 2, and 3). Zinc and Ni proved to catalyze the

formation of both crystalline and amorphous LDH minerals, with Zn forming crystalline

zaccagnaite and Ni forming amorphous LDH, indicated by the XRD spectra. In the SiO_2

systems, neither Mg or Zn induced the formation of new precipitates, but when SiO_2 was reacted

with Ni, a silicated-$Ni(OH)_2$ was formed. The presence of Si in the mixed oxide systems often

inhibited the formation of bayerite but did not inhibit the formation of LDH minerals, which

subsequently became silicated. Thus, in the reacted systems, K has the opportunity to intercalate

in the interlayer spaces of newly formed silicated LDH and hydroxide minerals.

The Al_2O_3 appears to be a more reactive mineral than SiO_2 in terms of changes in

mineralogy over time as denoted by the appearance of new peaks in the presence of Mg (Figure

1). However, the mixed oxide mineral system also presented new (yet smaller) peaks that were

attributed to bayerite. Over time, the intensity of those peaks increased, indicating a continuous

change in mineralogy. The presence of SiO_2 and thus dissolved Si inhibited the formation of

bayerite as indicated by the smaller peaks in the mixed oxide system (Figure 1). Additionally, the

presence of Mg appears to have inhibited the formation of bayerite in the mixed oxide system.

3.2 Linking adsorption to changes in mineralogy

In general, all mineral systems indicated that the amount of K adsorbed was time

dependent. For the 1-week system, SiO_2 reacted with Zn (SiZn1W) had the greatest amount of K

adsorbed, and Al_2O_3 reacted with Mg (AlMg1W) had the least amount of K adsorbed (Table 1).

Similarly, for the 1-month systems, SiO_2 reacted with Ni (SiNi1M) had the highest amount of K

adsorbed, and Al_2O_3 reacted with Zn (AlZn1M) had the least amount of K adsorbed. In the single

mineral systems reacted for 1-week, Zn enhanced K adsorption more than other cations (e.g. q =

542 and 930 mg kg^{-1} in AlZn and SiZn system, respectively). Whereas, Ni seemed to enhance K

adsorption when these single systems were reacted for 1-month (e.g. q = 475 and 1282 mg kg^{-1} in

AlNi and SiNi). In the mixed mineral systems (Al_2O_3 + SiO_2) both reacted for 1-week and 1-

month, the addition of different cations displayed minimal effect on K adsorption, with q values

ranging from 617 to 909 mg kg^{-1}.

While AlMg1W contained the lowest amount of K sorbed to the surface (171 mg kg^{-1}),

an increase of 145% K sorption occurred when the reaction time was increased from 1-week to

1-month. This indicates that reaction time plays an important role in K sorption. In the SiMg

systems, K sorption increased by 22% over time, but not as much as in the AlMg system.

Similarly, in SiAl systems with no cations present, sorption increased by about 21% from 1-week

to 1-month. In addition to the reaction time, the type of mineral sorbent used also played a

significant role in increasing or decreasing K adsorption. For example, at the 1-week and 1-

month reaction times, the SiMg system sorbed significantly higher K than the AlMg system

(about 100% and 300%, respectively). There is no significant change in K sorption for the mixed SiAlMg system over time (748 to 776 mg kg^{-1}). Additionally, the mixed SiAlMg system sorbed slightly less K (748 mg kg^{-1}) than the single SiMg system (845 mg kg^{-1}). This difference could partially be attributed to slightly smaller surface area of the Al oxide 400 m^2 g^{-1} versus the Si oxide 640 m^2 g^{-1}. However, the surface area of these sorbents are not expected to remain constant throughout the entire reaction period as the XRD results (Section 3.1) indicated the formation of new minerals over time in several of the systems.

The addition of Zn compared to Mg in the Al systems enhanced K sorption during 1-week reaction period (AlZn versus AlMg) by increasing the K sorption from 171 to 542 mg kg^{-1}, which is over a 200% increase. However, this effect was not long-term because the 1-month samples decreased in K sorption down to 280 mg kg^{-1}. This decrease could be attributed to the formation of positively charged layered double hydroxides in the AlZn systems, which repels positively charged K ions. The presence of Ni increased K sorption by 13.6% compared to that of Mg during the 1-month reaction time (AlNi1W versus AlMg1W). Overall, in single Al systems, the highest K sorption was found in Ni 1-month and Zn 1-week reaction times. This suggests that the formation of new mineral precipitates could enhance K sorption.

Of the three mineral systems, the Al systems adsorbed the least amount of K versus the Si and mixed SiAl system. In the Al systems, the average K sorption (including all cations) was 348 mg kg^{-1}. The Si system sorbed on average about 913 mg kg^{-1}, which is 162% of total K applied. The addition of γ-Al$_2$O$_3$ decreased average K sorption to 751 mg kg^{-1}. In the Si system, the presence of Ni resulted in the greatest K sorption among the three cations. There was an increase of 52% and 22% in K sorption compared to Mg and Zn, respectively. Based on the XRD results (Section 3.1), the increase in K sorption in the SiNi system may be due to the formation of Ni

phyllosilicate. In the mixed SiAl system, the presence of Zn, Mg, and Ni did not enhance K

sorption compared to the system with no additional cations (633, 748, 909, and 898 mg kg^{-1}

respectively). In fact, Zn and Mg resulted in 42% and 20% less K sorption than when they were

absent. This indicates that whether or not newly formed precipitates were formed, such as in the

Ni and Zn system, K sorption is also affected by the competitive sorption between K and other

dissolved cations (such as the background electrolyte or perhaps the buffer).

3.2.1 The effects of silicate

Overall, the greater K adsorption in Si systems could be attributed to several factors.

Firstly, Al and Si oxide minerals have different points of zero charge (PZC). The PZC for

gamma alumina is typically 8.5-10 [34] while that for SiO_2 is much lower (ca 2.0) [23]. Thus, the

surface charge of the SiO_2 is much lower than the Al_2O_3, which is one reason that SiO_2 has a

higher adsorption capacity for cations than Al_2O_3. Secondly, dissolved Si plays an important

role in stabilizing Al-rich and other metal-rich surface precipitates [14, 35]. This can stabilize

hydroxide sheets and the resulting >SiOH surface functional groups can act as additional

sorption sites. The presence of Si seems to enhance K adsorption due to the formation of

silicated, layered minerals. For example, in the AlZn system K adsorption decreased in the

absence of Si; however, when Si was added to this system, an increase in K adsorption was

found (Table 1). These aqueous values may indicate that K can potentially become incorporated

in interlayer spaces of silicated LDH.

To further clarify the role of Si on K adsorption, we calculated surface area normalized K

adsorption values from the 50:50 mixed system. These systems with both Al and Si oxides

indicated greater K adsorption values than the predicted theoretical values (Table 2), indicating a

synergistic effect of Al and Si on K adsorption. A higher K sorption density than expected was

found in all SiAl systems, except for SiAlZn system, indicating that the role of dissolved Si on K

adsorption seems to be important in the Mg and Ni systems on a short-time scale and less so for

the Zn systems (Table 2). Theoretical sorption densities were calculated from the equal masses

(0.05 g) of each metal oxide mineral and the surface area of those minerals. When the differences

between observed and theoretical surface area normalized sorption densities were averaged, a

31% increase in K adsorption in the presence of Si was observed. This increase in K sorption

beyond the expected amount indicates that surface precipitation and dissolved silicate can play

an important role to enhance K removal from the solution.

Furthermore, the addition of other cations not only affected the extent of K adsorption but

also affected the dissolved concentration of Si and Al. In the Al system, the concentration of

dissolved Al in solution decreased in all experimental reactions when reaction time was

increased from 1-week to 1-month. This indicates that Al precipitation continue to occur over

time. The amount of dissolved Al was lower in the presence of Zn by 175% and 275% compared

to Ni and Mg, respectively. This is likely due to the hydrolysis of Al and re-incorporation into

either bayerite or newly formed LDH solids.

In the mixed mineral systems at 1-week, the dissolved Al was similar in both the

presence and absence of Mg, whereas at 1-month, the dissolved Al was greater in the presence of

Mg than when no Mg was present (0.539 versus 0.228 mg L^{-1}) indicating that Mg did not

enhance Al precipitation and also likely did not enhance the formation of surface precipitates. It

appears that Mg inhibited the formation of Al-rich precipitate (bayerite). This result is supported

by the XRD patterns, where bayerite peaks can be observed when no Mg is present and there is a

lack of bayerite peaks in presence of Mg. Thus, the lower amounts of dissolved Al in the absence

of Mg is likely because the Al is being removed from solution and reprecipitated as bayerite.

However, when Zn and Ni were added at 1-month, the dissolved Al decreased by 48% and 29%, respectively. This implies that in the presence of Zn and Ni, more Al is involved in precipitate formation.

In the systems with only Si, the presence of Zn and Ni also decreased dissolved Si. This was most noticeable with the 1-week Zn sample (SiZn1W). Dissolved Si levels remained high in Mg versus the Ni systems (39.4 mg L^{-1} vs 34.9 mg L^{-1} vs). The XRD result (Section 3.1) indicates the formation of a Ni phyllosilicate in both the 1-week and 1-month samples, which justifies the presence of low dissolved Si in those samples. With the presence of Al, a much higher amount of Si binds to the solids and is removed from the solution. The average dissolved Si in the absence of γ-Al$_2$O$_3$ was greater (31 mg L^{-1}) than in the presence of γ-Al$_2$O$_3$ (1 mg L^{-1}). This indicates that the additional Si oxides surfaces were important binding site for dissolved Al. A specific example of loss of Si from solution and its potential re-adsorption to Al solids is in comparison of the SiMg, SiAlMg, and SiAl systems. SiMg has much higher dissolved silicon in solution versus when Al is added to the system in SiAlMg and SiAl (ca 38 mg/L vs ca <1 mg/L). This loss of dissolved silicon in the presence of Al oxide indicates that the dissolved silicon is complexing with Al and being removed from solution.

3.2.2 Satisfying surface precipitate charge

The results from K sorption experiments suggest that time can significantly affect K adsorption; longer reaction time generally caused more K to be bound on the solid. This is particularly true in the AlMg, SiMg, SiAl, SiZn, AlNi, SiNi, and SiAlNi systems (Table 1). Some of the changes in K adsorption could be attributed to the formation of new surface

precipitates. For example, K adsorption can either increase or decrease depending on the type of

surface precipitate. A decrease in K adsorption is evident over time e.g., in the AlZn system; this

change is likely due to the formation of positively charged surface precipitates. XRD data also

indicates that among the SiMg, SiZn, and SiNi systems, only with SiNi did a newly formed

precipitate occur. The SiNi1M sample also has the highest q value (1282 mg kg^{-1}), indicating

that the formation of the silicated $Ni(OH)_2$ may be responsible for retaining more K. This trend is

less evident in the 1-week reaction period.

On the other hand, the XRD data indicated a dramatic formation of crystalline LDH

(zaccagnaite) in the AlZn systems. This mineral is well known to have positive charge, and thus

its formation will inhibit K adsorption in interlayer spaces as K is positively charged. However,

in the mixed oxide system, a large presence of LDH was also clearly indicated by the XRD, and

the formation of LDH was not inhibited by the presence of Si. The dissolved Si (H_4SiO_4) will

satisfy the positive charge of the newly formed LDH by intercalating and binding to the

hydroxide sheet; dissolved Si is well known to replace anions in the interlayer spaces of LDH to

form thermodynamically stable silicated LDH [15].

In the Ni systems, the generation of new precipitates occur in all three sorption reactions

(AlNi, SiNi, and SiAlNi). Although the presence of LDH and bayerite are detected in the AlNi

system, the decrease in K sorption is not observed here as in the AlZn system. This is perhaps

due to the smaller presence of surface precipitates and generally more amorphous structure as

noted in the peaks in the AlNi system.

3.3 Variations in pH

The pH value of the samples ranged from 8.29 to 8.77 (Table 3) during the 1 week and 1 month reaction period. The initial pH of the unreacted slurry was 8.50. However, in presence of Zn and Ni, pH initially dropped to 8.37 and 8.40 (Table 3) during 1-week of reaction. This indicates that the hydrolysis of cations was occurring, during which a proton is released resulting in lower pH values. This drop in pH was not apparent in any of the single or mixed systems when Mg was present. In fact, the pH values slightly increased to 8.55 when Mg was present in these systems and increased to 8.59 when no additional cations were added. When both sorbent and additional cations were absent, the pH increased to up to 8.77 during both reaction times. In general, the drop in pH value was most pronounced in the samples with Zn and Ni during both reaction periods; whereas, the presence of Mg resulted in solutions with the highest pH values. This result can be expected as Mg has slower hydrolysis rate than Ni and Zn.

In general, the longer the samples reacted, the more acidic the solutions became (e.g., the pH dropped by 0.04 to 0.20 units). The presence of Mg seems to have the least effect on pH over time; the pH decreased by only 0.04 to 0.06 units. Samples with Ni were observed to have the largest decrease in pH (0.07 to 0.09 units), which is slightly greater than the decrease in pH for Zn samples. The decrease in pH is expected to be larger with the addition of transition metals than with Mg due to hydrolysis of transition metals. Silicon oxides samples resulted in a slightly lower pH than Al_2O_3 samples. Samples without minerals or cations tend to have greater pH. The samples with oxide minerals and cations were more reactive and became more acidic.

3.4 Potassium surface adsorption species

While XRD is a useful technique to identify the phase/mineralogy of the sample, it does not provide information about the local coordination environment of K. Thus, we cannot

determine the binding environment of K adsorbed to the solid phase minerals (either surface

precipitates or starting materials); i.e., we cannot determine whether K is bound in the interlayer

spaces. However, K binding mechanisms can be established using synchrotron based XAS [18, 36-42]. We aim to determine if K can be bound to surface precipitates and compare different binding

mechanisms of K onto Al and Si oxides using XANES. Potassium K-edge XANES data are

shown in Figures 4 and 5, and Table S1 tabulates the XANES spectral features located at

different energy positions. Figure 4a is an overview plot of all the samples reacted for 1-month

and several samples reacted for 1-week. In general, the position of the white line in all sample

spectra was constant but depending on both reaction time and cations present, different shoulder

features were observed on the white line, the peak of the white line, and in the post-edge region

(Figure 4b). The formation of a post-edge peak in the Al system is highlighted in Figure 5a,

particularly in the inset. Comparisons of K sorption in the Si system and the mixed SiAl system

are shown in the Figure 5b and 5c, respectively.

In the AlMg1M sample (Figure 4a), the pre-edge region between 3605-3609 eV

displayed no significant features. A slight shoulder feature occurs on the upslope of the edge step

at 3610.7 eV and the peak of the white line is at 3615.4 eV. There was no shoulder feature

formed on the downward slope of the white line. The peak dropped steeply and formed a valley

at 3624.5 eV. The first post-edge peak is observed at 3628.4 eV. This peak is distinct from other

reaction systems, indicating that K sorption mechanism is different here than in the SiAl and Si

systems. The peak at 3628.4 eV is followed by a valley at 3632.4 eV. The largest post-edge peak

is present at 3643.4 eV. No significant features can be observed beyond this point.

When comparing the AlMg1M to AlMg1W (Figure 4a), the shoulder feature in 1M

spectra showed a 0.3 eV shift to higher energy; the 1W sample showed a slight shoulder at

3610.4 eV. In addition, the amplitude of the white line is less intense in the 1W sample compared to the corresponding 1M sample. The 1W white line peak is slightly shifted to the higher energy at 3616 eV as opposed to the 1M sample at 3615.4 eV. An important distinction between the 1W and the 1M samples is that the peak after the white line at 3628.4 eV is subtle (less intense) than the peak in the 1M sample (Figure 5a). This indicates that the longer the samples react, the more intensified the peak becomes, suggesting that the K sorption complex changes over time. Typically, more significant scattering features are found for atoms that are more highly coordinated. Higher amplitudes for the white line at 3615.4 eV and the largest post-edge peak at 3543.4 eV are also observed for 1M samples. The increase of the peak amplitudes with time indicates that the coordination of K with other elements increases with time. As it can be seen in the XRD pattern of the samples (Figure 1), the 1M sample has more intense peak of bayerite formed as a surface precipitate. Therefore, the increase in K coordination with time may be related to its inclusion in the interlayer space of the newly formed bayerite. In the Al system, time plays an important role in modifying K coordination.

With respect to the AlZn1M and AlNi1M, similar shoulder features on the upslope of the white line were found at 3610.5 eV and 3610.4 eV, respectively. The peak of the white line for AlZn1M is observed at around 3615.4 eV. The following post-edge peaks and valleys are present in similar energy positions as that of the AlMg1M sample. The intensities of AlZn1M and AlNi1M peaks at 3628.4 eV are lower than that of AlMg1M. This implies that K is more coordinated to bayerite in presence of Mg than in presence of Ni and Zn (Figures 1 and 3). Furthermore, an additional subtle shoulder was observed at 3612.2 eV in AlNi1M, which was absent in Mg and Zn containing Al samples. The AlZn system is particularly challenging to analyze because it contains the presence of both bayerite and zaccagnaite surface precipitates. In

the AlZn system, K sorption decreases even though bayerite peaks increase (as indicated by q

values and XRD, respectively). In AlMg system, however, K sorption increases and bayerite

peaks increase (as indicated by q values and XRD, respectively). Because both of these surface

precipitates are actively forming, there is potentially a competition for sorption between newly

formed LDH and newly formed bayerite.

Apart from the sorption reaction of K in the Al systems, K sorption in the Si systems

presented several unique features in the XANES spectra. The presence of a small shoulder

feature at 3614 eV in the white line region can be observed in the SiMg1M compared to the

SiMg1W sample. The presence of the enhanced shoulder feature again indicates that the longer

the reaction time, the more coordinated K becomes; this was also observed for the Al system. For

SiZn1M and SiMg1M sample, the spectra showed more defined features than that of Ni. The Zn

and Mg samples showed a shoulder at 3614 eV, whereas that feature is absent in Ni sample

(Figure 5b). However, XRD data from the SiNi systems indicates the formation of silicated Ni-

hydroxide minerals. While the XRD data helps to identify the formation of newly formed

minerals, often these minerals are poorly crystalline and difficult to be identified by the XRD.

The lack of the shoulder feature at 3614 eV indicates that the K sorption mechanism is different

in the presence of layered silicated hydroxide minerals. Perhaps, in the SiMg and SiZn systems,

K is adsorbed to the surface of SiO_2, while K is incorporated into the interlayer space in the SiNi

systems. When K is incorporated in larger interlayer spaces, such as those found in

montmorillonite, the XANES spectra tend to have fewer features [26]. Regardless, the position of

the white line for all three samples (SiZn1M, SiMg1M, SiNi1M) is at the same energy, i.e, at

3616 eV.

In the mixed system of SiAl with no additional cations (besides K), the spectra of 1M and 1W samples show no difference except for a shoulder at 3610.8 eV in the 1W sample and the higher intensity of the white line in the 1M sample. The shoulder feature is more defined in the 1M sample perhaps due to increased K coordination over time; however, the concentration of K bound to the solid varies only by 21% (742 mg kg^{-1} vs 898 mg kg^{-1}). The SiAlMg samples for both 1W and 1M present shoulder features at 3610.8 and 3613.7 eV. Noticeably, the second shoulder at 3613.7 eV and the peak of the white line at 3616 eV are less intense in the 1W than the 1M sample. In the SiAl systems (Figure 5c) with Mg, Zn, Ni, and no additional cation, all samples had shoulder features at 3610.9 eV and 3613 eV and the white line position at 3616 eV. The white line intensity of the Zn sample was the highest followed by Ni, Mg, and the no cation sample. For the SiAlZn1M sample, the intensity of the first post-edge valley was higher than the other mixed samples, but the first post-edge peak overlapped with other samples in the region between 3634 and 3656 eV.

When considering the XANES spectra from the SiAl systems (Figure 5c) and comparing it to the XRD data (Figure 1, 2, and 3), it is important to note that while XRD indicates the formation of bayerite, ZnAl LDH, and silicated Ni(OH)$_2$ (in the no cation, Zn, and Ni systems, respectively), that these new minerals do not appear to significantly alter the XANES spectra. This indicates that K speciation in the four different systems (which have different mineralogy) is broadly similar, where K is likely complexed to the solid via outer sphere-surface complexation. The potential binding of K in newly formed interlayer spaces is difficult to identify when K is bound via outer-sphere complexation, even if it is located in the interlayer region. Perhaps, in the SiAlMg1M sample, the shoulder feature at 3613 eV is somewhat

enhanced, but it is difficult to distinguish that particular feature from potential noise in the spectra.

While reaction times and the presence of different cations both affected K adsorption (as discussed above), the adsorbent (i.e., the solid phase) also impacted K speciation, as indicated in Figure 5d. The first post-edge peak is evident in the XANES data between 3624 and 3634 eV for Al samples reacted with Zn and Mg, and there is also a small peak at the same location in the AlNi sample as well. However, this peak is completely absent in all of the Si samples. This peak may be related to inner-sphere surface complexation of K to the Al-oxide surface. These results indicate that the binding mechanism of K to Si is different than that to Al oxides. However, the role of newly formed precipitates is still unclear. The XRD data indicate that SiO_2 reacted with Ni forms silicated $Ni(OH)_2$ that has interlayer space, while SiO_2 reacted with Mg and Zn do not seem to form such silicated hydroxides (Figure 1, 2, and 3). Whereas, all three cations (Ni, Zn, Mg) in the Al samples seem to catalyze the formation of new precipitates, including bayerite and LDH. X-ray diffraction results indicated that surface precipitates were formed in both AlNi and SiNi samples; however, the XANES spectra for these two samples show slightly different spectral features, where a subtle peak is present in the post edge region only in AlNi1M sample.

4. Conclusion and Future Directions

While the presence of newly formed precipitates is affecting K adsorption, the compositions of the solids themselves play a critical role. This is evident when considering wet chemical, X-ray diffraction, and XAS data. For example, much more K is adsorbed in the Si systems (e.g., 1054 and 1282 mg kg^{-1}) versus the Al systems (e.g., 280 and 475 mg kg^{-1}) in the presence of Zn and Ni, respectively. In the Al system, XRD indicates significant formation of

LDH and perhaps the presence of inner-sphere K complexation according to XANES spectra (Figure 5d). In addition to these changes, silica appears to have an additional role for the enhancement of K adsorption. The presence of Si seems to enhance K adsorption due to potentially two different factors: (1) its role in the formation of silicated, layered minerals, where it stabilizes metal hydroxides, or (2) the creation of additional surface site (>SiOH) which effectively increases the number of sorption site available for K binding. These aqueous values, particularly for Zn, may indicate that K can potentially become incorporated in interlayer spaces of silicated LDHs. Lastly, the surface area normalized K adsorption values indicated that on average the mixed oxide systems had 31% additional K adsorption beyond the predicted values over our experimental time periods.

While these adsorption studies and the formation of new precipitates provide important evidence for the increased adsorption of K, the stability of K on these mineral surfaces is not clear. Thus, additional studies on K desorption are necessary, particularly in the presence of other common co-ions such as Ca^{2+}, which is a common component of the soil solution. Additional future experiments include longer reaction times, e.g., 1 year, to identify maximum K sorption to the solids. Also, utilizing dissolved silica versus SiO_2 may provide improved insight into the role of silica for neutralizing the positively charged LDH and providing additional acid sorption sites. Further investigation using EXAFS spectroscopy will clarify if K is bound via outer-sphere or inner-sphere surface complexation to newly formed minerals.

Conflicts of interest:

There are no conflicts of interest to declare.

References

1. V. Ambroise, S. Legay, G. Guerriero, J.-F. Hausman, A. Cuypers and K. Sergeant, *Plant and Cell Physiology*, 2019, **61**, 3-20.
2. C. H. Suelter, in *Potassium in Agriculture*, 1985, DOI: https://doi.org/10.2134/1985.potassium.c13, pp. 337-349.
3. X. Xu, X. Du, F. Wang, J. Sha, Q. Chen, G. Tian, Z. Zhu, S. Ge and Y. Jiang, *Frontiers in Plant Science*, 2020, **11**.
4. K. Tanaka, S. Gilroy, A. M. Jones and G. Stacey, *Trends in Cell Biology*, 2010, **20**, 601-608.
5. A. N. Shahzad, M. Rizwan, M. G. Asghar, M. K. Qureshi, S. A. H. Bukhari, A. Kiran and A. Wakeel, *Scientific Reports*, 2019, **9**, 7378.
6. I. L. B. Pabuayon, K. L. Lewis and G. L. Ritchie, *Agronomy Journal*, 2020, **112**, 4373-4385.
7. N. Y. O. Kusi, K. L. Lewis, G. D. Morgan, G. L. Ritchie, S. K. Deb, R. D. Stevens and H. Y. Sintim, *Agronomy Journal*, 2021, DOI: https://doi.org/10.1002/agj2.20807.
8. D. M. Oosterhuis, D. A. Loka and T. B. Raper, *Journal of Plant Nutrition and Soil Science*, 2013, **176**, 331-343.
9. C. A. Rosolem and D. S. Mikkelsen, *J. Plant Nutr.*, 1991, **14**, 1001-1016.
10. N. J. Volk, *Soil Sci.*, 1934, **37**, 267-288.
11. D. L. Sparks and P. M. Huang, in *Potassium in Agriculture*, 1985, DOI: https://doi.org/10.2134/1985.potassium.c9, pp. 201-276.

12. R. D. Munson, ed., *Potassium in Agriculture*, ASA-CSSA-SSSA, 1985.

13. M. G. Siebecker, W. Li and D. L. Sparks, in *Advances in Agronomy*, ed. D. L. Sparks, Academic Press, 2018, vol. 147, pp. 1-59.

14. X. Mo, M. G. Siebecker, W. Gou and W. Li, *Geochim. Cosmochim. Acta*, 2021, **314**, 85-107.

15. E. Peltier, R. Allada, A. Navrotsky and D. L. Sparks, *Clays and Clay Minerals*, 2006, **54**, 153-164.

16. R. L. Malcolm and V. C. Kennedy, *Soil Science Society of America Journal*, 1969, **33**, 247-253.

17. D. L. Sparks and P. M. Jardine, *Soil Science Society of America Journal*, 1981, **45**, 1094-1099.

18. V. Vao-soongnern, C. Pipatpanukul and S. Horpibulsuk, *Journal of Materials Science*, 2015, **50**, 7126-7136.

19. J. A. Kittrick, *Soil Science Society of America Journal*, 1966, **30**, 801-803.

20. M. Siebecker, W. Li, S. Khalid and D. Sparks, *Nature Communications*, 2014, **5**, 5003.

21. A. C. Scheinost and D. L. Sparks, *Journal of Colloid and Interface Science*, 2000, **223**, 167-178.

22. A. M. Scheidegger, G. M. Lamble and D. L. Sparks, *Journal of Colloid and Interface Science*, 1997, **186**, 118-128.

23. D. L. Sparks, *Environmental Soil Chemistry*, Academic Press, San Diego, 2nd. edn., 2002.

24. W. Li, K. J. T. Livi, W. Xu, M. G. Siebecker, Y. Wang, B. L. Phillips and D. L. Sparks, *Environmental Science & Technology*, 2012, **46**, 11670-11677.

25. Q. Sun, C. Liu, P. Cui, T. Fan, M. Zhu, M. E. Alves, M. G. Siebecker, D. L. Sparks, T. Wu, W. Li, D. Zhou and Y. Wang, *Environ. Int.*, 2019, **126**, 234-241.

26. E. J. Schmidt, G. Zanoni, A. Bumguardner, B. Šegvić, K. Lewis, D. Abdala and M. G. Siebecker, *Geoderma*, 2022, **422**, 115914.

27. G. Cibin, A. Mottana, A. Marcelli and M. F. Brigatti, *Mineralogy and Petrology*, 2005, **85**, 67-87.

28. B. Ravel and M. Newville, *Journal of Synchrotron Radiation*, 2005, **12**, 537-541.

29. S. M. Webb, *Physica Scripta*, 2005, DOI: 10.1238/physica.topical.115a01011, 1011.

30. S. Merlino and P. Orlandi, *American Mineralogist*, 2001, **86**, 1293-1301.

31. K. J. T. Livi, G. S. Senesi, A. C. Scheinost and D. L. Sparks, *Environ. Sci. Technol.*, 2009, **43**, 1299-1304.

32. T. P. Trainor, G. E. Brown and G. A. Parks, *Journal of Colloid and Interface Science*, 2000, **231**, 359-372.

33. W. Gou, M. G. Siebecker, Z. Wang and W. Li, *Geochem. Trans.*, 2018, **19**, 9.

34. M. Kosmulski, *Advances in Colloid and Interface Science*, 2020, **275**, 102064.

35. E. Peltier, R. Allada, A. Navrotsky and D. L. Sparks, *Clays Clay Miner.*, 2006, **54**, 153-164.

36. M. F. Brigatti, D. Malferrari, M. Poppi, A. Mottana, G. Cibin, A. Marcelli and G. Cinque, *American Mineralogist*, 2008, **93**, 821-830.

37. C. J. Davies, A. Mayer, J. Gabb, J. M. Walls, V. Degirmenci, P. B. Thompson, G. Cibin, S. Golunski and S. A. Kondrat, *Phys. Chem. Chem. Phys.*, 2020, **22**, 18976-18988.

38. G. Jacobs, V. R. R. Pendyala, M. Martinelli, W. D. Shafer, M. K. Gnanamani, S. Khalid, A. MacLennan, Y. Hu and B. H. Davis, *Catalysis Letters*, 2017, **147**, 1861-1870.

39.   W. O. Santos, E. M. Mattiello, A. A. Pacheco, L. Vergutz, L. F. da Silva Souza-Filho and D. B. Abdala, *International Journal of Mineral Processing*, 2017, **159**, 16-21.
40.   W. Xu, D. Chen, W. Chu, Z. Wu, A. Marcelli, A. Mottana, A. Soldatov and M. F. Brigatti, *Journal of synchrotron radiation*, 2011, **18**, 418-426.
41.   W. Li, X. M. Liu and Y. Hu, *Geostandards and Geoanalytical Research*, 2020, **44**, 805-819.
42.   A. Sharma and D. Hesterberg, in *Multidimensional Analytical Techniques in Environmental Research*, eds. R. Duarte and A. Duarte, Elsevier, 2020, ch. 9 - Synchrotron radiation-based spatial methods in environmental biogeochemistry, pp. 231-265.

Table 1. *The amount of K sorbed to the solids (q in mg kg^{-1}) and the dissolved concentrations of other ions in solution (mg L^{-1}).*

Abbreviation	Sample description	q (K)	K	Al	Ni	Si	Zn
AlMg1W	Al_2O_3 reacted with Mg for 1W	171 ± 52	35.1 ± 0.1	0.385 ± 0.011			
AlMg1M	Al_2O_3 reacted with Mg for 1M	418 ± 669	34.2 ± 1.6	0.182 ± 0.001			
SiMg1W	SiO_2 reacted with Mg for 1W	695 ± 157	33.5 ± 0.3			37.6 ± 1.5	
SiMg1M	SiO_2 reacted with Mg for1M	845 ± 38	33.1 ± 0.1			39.4 ± 1.6	
SiAlMg1W	SiO_2+Al_2O_3 reacted with Mg for 1W	776 ± 140	33.3 ± 0.3	0.56 ± 0.026		0.637 ± 0.05	
SiAlMg1M	SiO_2+Al_2O_3 reacted with Mg for 1M	748 ± 240	33.3 ± 0.5	0.539 ± 0.022		0.911 ± 0.07	
SiAl1W	SiO_2+Al_2O_3 reacted with no cation for 1W	742 ± 115	33.3 ± 0.3	0.577 ± 0.008		0.592 ± 0.04	
SiAl1M	SiO_2+Al_2O_3 reacted with no cation for 1M	898 ± 255	33.0 ± 0.6	0.228 ± 0.015		1.02 ± 0.05	
Mg1W	No mineral reacted with Mg for 1W		34.3 ± 0.1				
Mg1M	No mineral reacted with Mg for 1M		33.6 ± 0.2				
AlZn1W	Al_2O_3 reacted with Zn for 1W	542 ± 14	33.8 ± 0.1	0.105 ± 0.002			0.036 ± 0.001
AlZn1M	Al_2O_3 reacted with Zn for 1M	280 ± 139	34.5 ± 0.3	0.049 ± 0.005			0.040 ± 0.001
SiZn1W	SiO_2 reacted with Zn for 1W	930 ± 107	32.9 ± 0.1			15.9 ± 0.7	0.485 ± 0.004
SiZn1M	SiO_2 reacted with Zn for 1M	1054 ± 54	32.7 ± 0.1			27.0 ± 1.4	0.283 ± 0.018
SiAlZn1W	SiO_2+Al_2O_3 reacted with Zn for 1W	617 ± 67	33.7 ± 0.1	0.069 ± 0.005		1.0 ± 0.1	0.072 ± 0.004
SiAlZn1M	SiO_2+Al_2O_3 reacted with Zn for 1M	633 ± 156	33.6 ± 0.3	0.119 ± 0.004		1.06 ± 0.08	0.043 ± 0.002
AlNi1W	Al_2O_3 reacted with Ni for 1W	203 ± 144	34.7 ± 0.3	0.204 ± 0.001	0.037 ± 0.003		
AlNi1M	Al_2O_3 reacted with Ni for 1M	475 ± 164	34.0 ± 0.3	0.133 ± 0.001	0.040 ± 0.001		
SiNi1W	SiO_2 reacted with Ni for 1W	673 ± 147	33.6 ± 0.3		0.029 ± 0.001	32.1 ± 1.3	
SiNi1M	SiO_2 reacted with Ni for 1M	1282 ± 587	32.1 ± 1.2		0.008 ± 0.001	34.9 ± 1.5	
SiAlNi1W	SiO_2+Al_2O_3 reacted with Ni for 1W	686 ± 136	33.5 ± 0.3	0.117 ± 0.009	0.034 ± 0.001	0.958 ± 0.081	
SiAlNi1M	SiO_2+Al_2O_3 reacted with Ni for 1M	909 ± 42	33.0 ± 0.1	0.162 ± 0.003	0.026 ± 0.002	1.12 ± 0.11	

Table 2. *Surface area-normalized K sorption densities. The observed and theoretical values for K sorption density onto Al and Si oxide surfaces were calculated based on mineral surface areas. Theoretical values are only calculated for mixed SiAl systems. The differences between the theoretical values and observed values highlights the influence of surface precipitates.*

Sample Name	Observed q (mg K kg^{-1})	Theoretical q (mg K kg^{-1})	Observed µg K/m^2	± observed (µg K/m^2)	Theoretical (µg K/m^2)	Observed nmol/m^2	Theoretical nmol/m^2
AlMg1W	171	-	0.43	0.13	-	10.9	-
AlMg1M	418	-	1.04	1.67	-	26.7	-
SiMg1W	695	-	1.09	0.25	-	27.8	-
SiMg1M	845	-	1.32	0.06		33.8	-
SiAlMg1W	776	432.8	1.49	0.27	0.76	38.2	19.3
SiAlMg1M	748	631.2	1.44	0.46	1.18	36.8	30.2
AlZn1W	542	-	1.36	0.03	-	34.7	-
AlZn1M	280	-	0.7	0.35	-	17.9	-
SiZn1W	930	-	1.45	0.17	-	37.2	-
SiZn1M	1054	-	1.65	0.08	-	42.1	-
SiAlZn1W	617	736	1.19	0.13	1.4	30.4	35.9
SiAlZn1M	633	667	1.22	0.3	1.17	31.1	30
AlNi1W	203		0.51	0.36		13	
AlNi1M	475		1.19	0.41		30.3	
SiNi1W	673		1.05	0.23		26.9	
SiNi1M	1282		2	0.92		51.2	
SiAlNi1W	686	438	1.32	0.26	0.78	33.8	19.9
SiAlNi1M	909	878	1.75	0.08	1.59	44.7	40.8

Table 3. *Average pH values measured for K adsorption experiments at 1-week and 1-month.*

Abbreviation	Sample	1-week	1-month	pH change from 1-week
AlMg	Al_2O_3 with Mg	8.56	8.51	-0.04
SiMg	SiO_2 with Mg	8.56	8.51	-0.05
SiAlMg	$Al_2O_3 + SiO_2$ with Mg	8.55	8.49	-0.06
AlZn	Al_2O_3 with Zn	8.38	8.33	-0.05
SiZn	SiO_2 with Zn	8.35	8.29	-0.06
SiAlZn	$Al_2O_3 + SiO_2$ with Zn	8.37	8.31	-0.06
AlNi	Al_2O_3 with Ni	8.40	8.33	-0.07
SiNi	SiO_2 with Ni	8.38	8.29	-0.09
SiAlNi	$Al_2O_3 + SiO_2$ with Ni	8.40	8.31	-0.09
Mg	No mineral with Mg	8.63	8.54	-0.09
SiAl	$Al_2O_3 + SiO_2$ (no cations: Mg, Ni, Zn)	8.59	8.55	-0.04
-	No mineral and no cations	8.77	8.55	-0.20

Figure 1. XRD of Al$_2$O$_3$ and SiO$_2$ reacted with K and Mg for 1-week and 1-month. DP signifies Dry Powder (non-reacted control samples). Peaks labelled as 'B' indicate bayerite and 'G' indicate gibbsite.
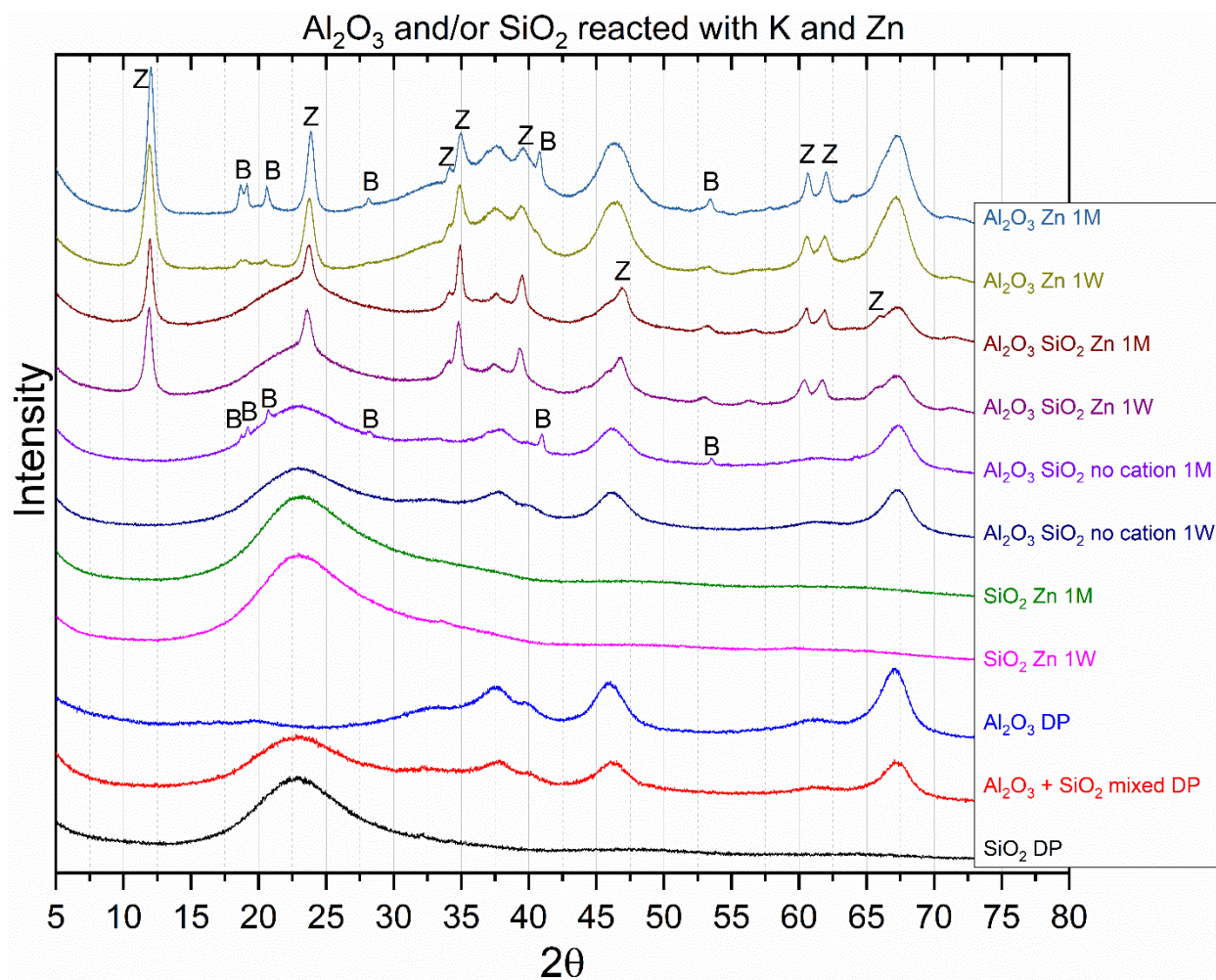
Figure 2. XRD of Al₂O₃ and SiO₂ reacted with K and Zn for 1-week and 1-month. DP signifies Dry Powder (non-reacted control samples). Peaks labelled as 'B' indicate bayerite and 'Z' indicate zaccagnaite.
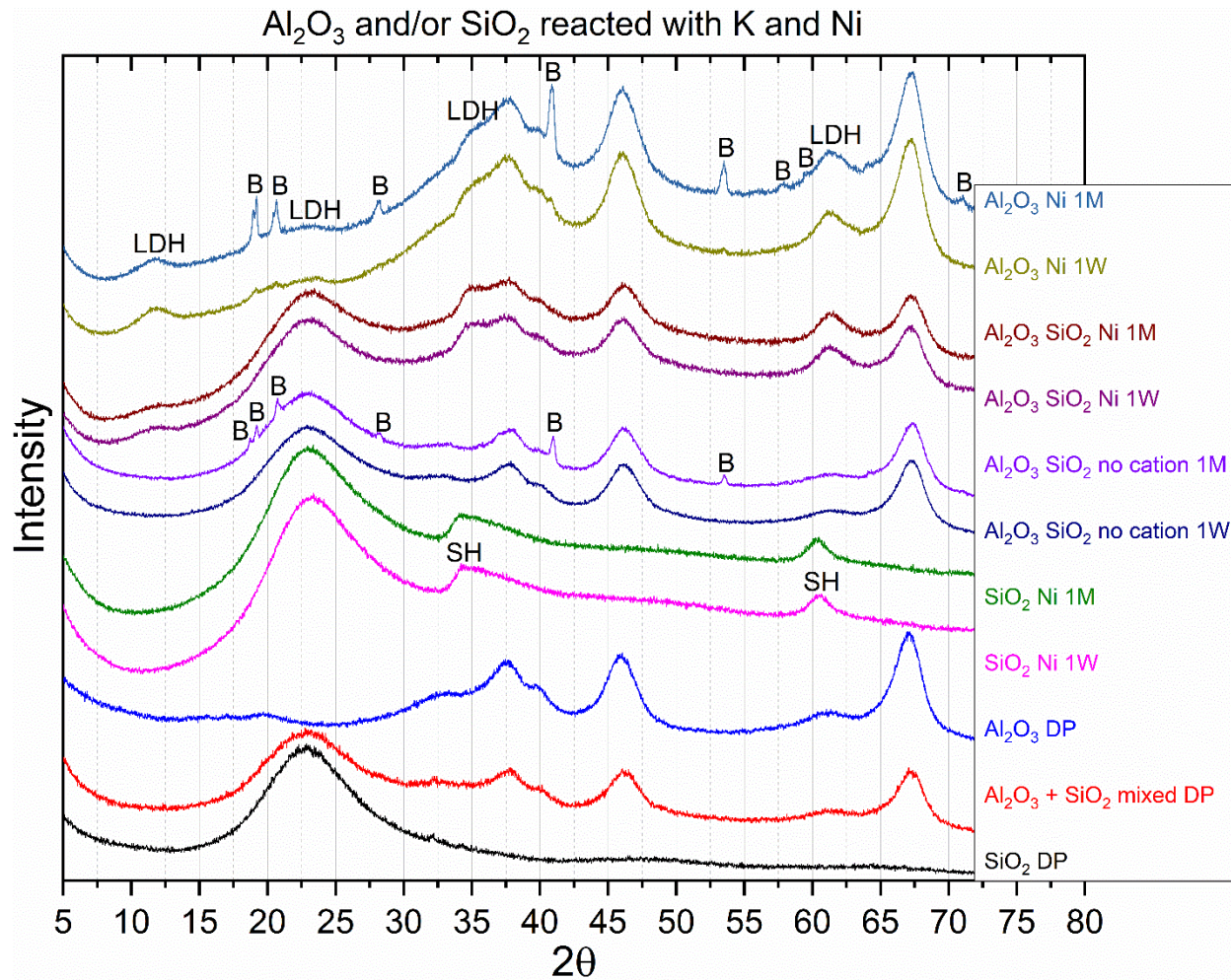
Figure 3. XRD of Al2O3 and SiO2 reacted with K and Ni for 1-week and 1-month. DP signifies Dry Powder (non-reacted control samples). Peaks label LDH = layered double hydroxide, B = bayerite, SH =silicated hydroxide.
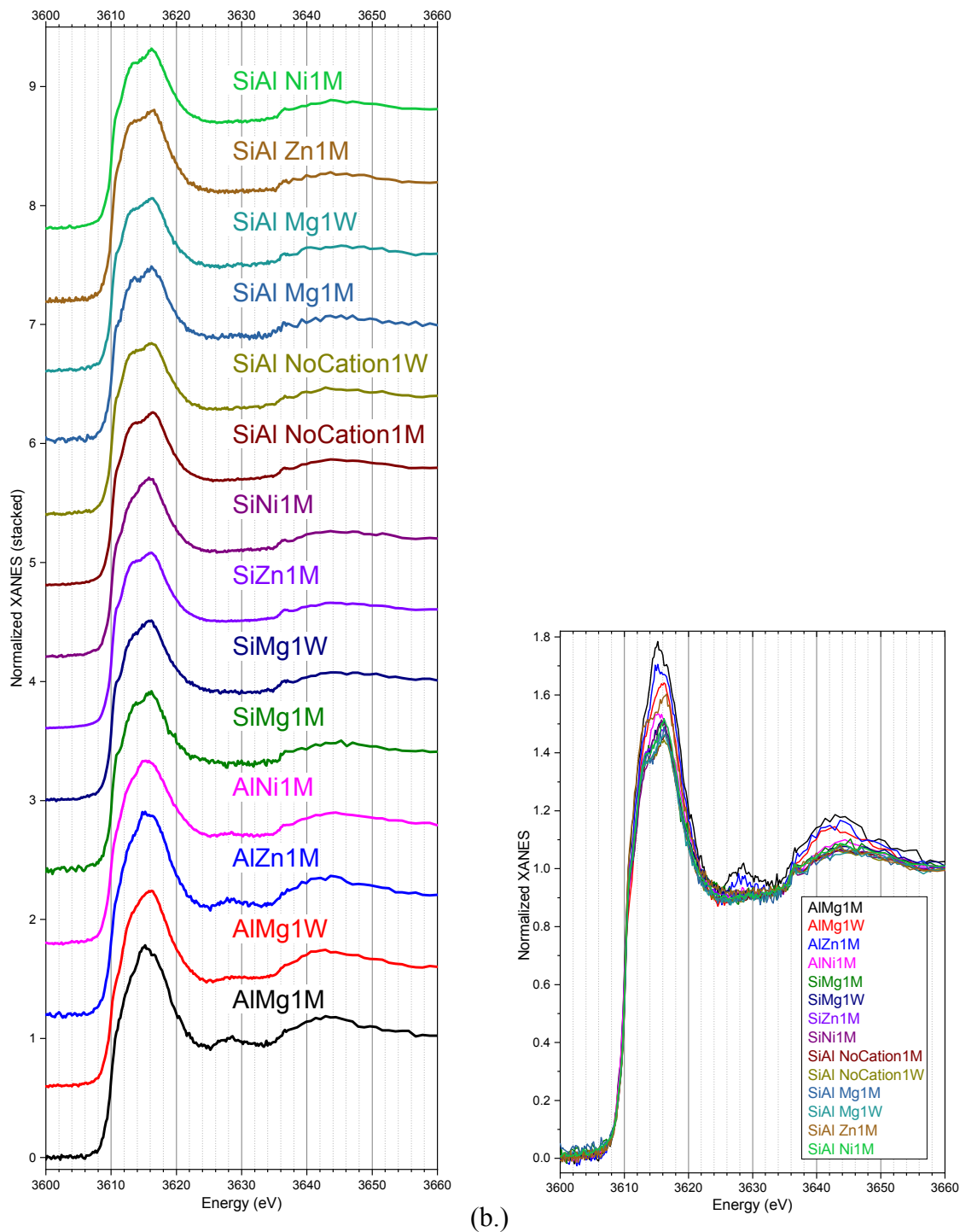
Figure 4. Potassium K-edge XANES spectra obtained from samples with different treatments. (a.) gives an overview of the sample spectra, and (b) facilitates the visualization of distinct features and helps to distinguish between different spectra.
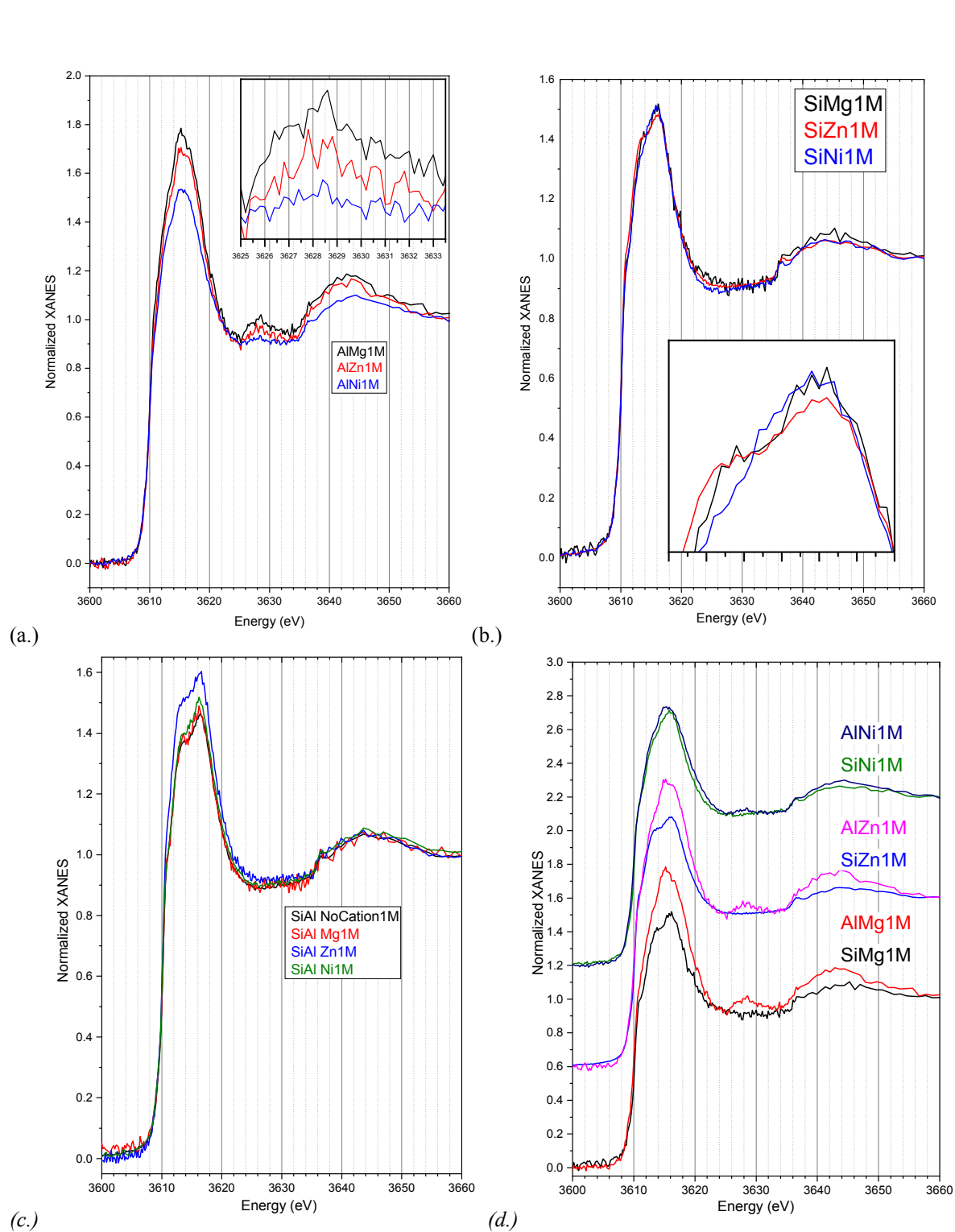
Figure 5. Potassium K-edge XANES data obtained from single Al systems (a), single Si systems (b), mixed SiAl systems (c) with different cations. Figure (d) shows the effect of each cation (Ni, Zn and Mg) on the single Al and Si systems.